Efficient Modelling and Optimization Approach for Grating-Based Flow Cytometers

A. C. A. Barzanji,[1,2,4] T. Ulrick,[1,2,3,4] K. Cools,[3,4] T. Reep,[1,2,4] N. Verellen[4], G. Yurtsever[4] and W. Bogaerts[1,2,4]

[1] Photonics Research Group, Ghent University – imec, 9502 Ghent, Belgium
[2] NB Photonics, Ghent University, 9052 Ghent, Belgium
[3] IDLab, Ghent University – imec, 9052, Ghent, Belgium
[4] IMEC, Kapeldreef 75, 3001 Heverlee, Belgium

This work presents a computationally efficient Transmission Matrix Model (TMM) for designing silicon nitride grating couplers in integrated flow cytometers. The TMM achieves a four to five orders-of-magnitude speed increase over Finite Difference Time Domain (FDTD) simulations, enabling fast, large-scale optimization. Incorporated into a Bayesian Optimization scheme, the TMM allows for optimization of transient Peak-to-Baseline (P2B) by the tuning of uniform and apodized grating configurations. A P2B transmission of 0.1389 is achieved for an optimized uniform grating and 0.2210 for a linearly apodized grating.

Introduction

Flow cytometry offers precise cell analysis but typically relies on large, expensive equipment. Integrated photonic systems seek to make this technology more accessible through miniaturization, though limited power collection efficiency in waveguides restricts cell detection sensitivity. Integrated optofluidic systems using grating couplers present a promising solution for efficient optical coupling. However, traditional numerical modeling methods like FDTD introduce significant computational demands, hindering rapid, iterative design optimization. This work presents a Transmission Matrix Model (TMM) that accurately simulates light transmission in a grating-based flow cytometry system, enabling integration with Bayesian Optimization to enhance optical coupling and detection sensitivity.

System Model

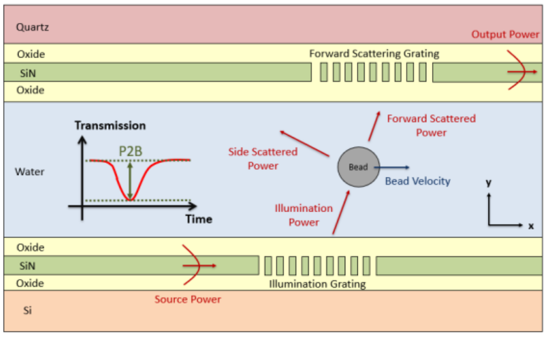

Figure 1 Schematic of the dynamic system power flow and transient transmission Peak to Baseline (P2B) as a bead travels through the channel.

The system illustrated in includes a microfluidic channel, 30 µm thick, positioned between silicon nitride waveguides with oxide cladding, as described by Jooken et al. [1], When illuminated by a 638 nm laser, an Illumination Grating (ILG) in the lower silicon nitride layer directs light across the microfluidic channel toward a Forward Scattering Grating (FSG) in the upper silicon nitride waveguide. As a polystyrene bead with a 3 µm radius (representing a biological cell) moves through the channel, it scatters light away from the FSG, resulting in a transient dip in FSG transmission.

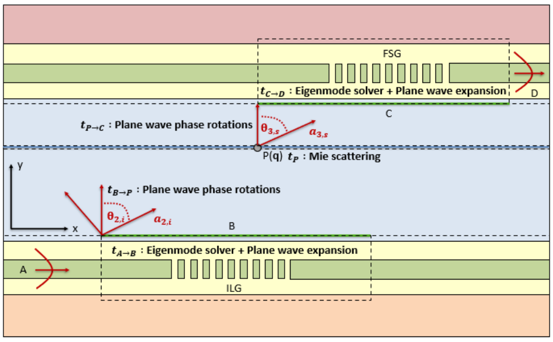

Figure 2 TMM modularization and matrix generation methods of the grating system with a bead P at a position 'q' in the microfluidic channel.

Optical power flow through the system can be modeled using a 2D TMM, treating the layers and components as linear, lossless dielectrics. The system is modularized into sub-components, each represented by coherent transmission matrices as in Figure 2. The matrix elements consist of upwards propagating plane waves, ignoring back reflections. Modal power transmission from A to D can be found by cascading the matrices using Eqn. 1, a computationally inexpensive operation.

$$T_{A\to D} = |\boldsymbol{t_{A\to D}}|^2 = |\boldsymbol{t_{C\to D}}.\boldsymbol{t_{P\to C}}.\boldsymbol{t_{P}}.\boldsymbol{t_{B\to P}}.\boldsymbol{t_{A\to B}}| \qquad (1)$$

Component Models

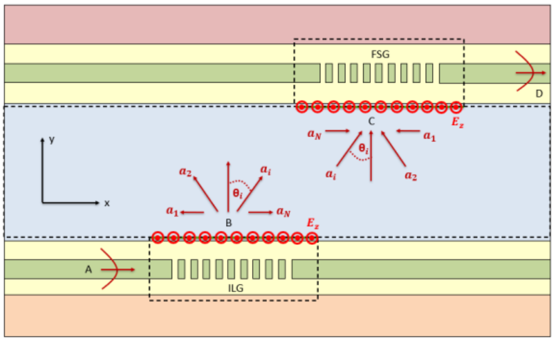

Figure 3 TMM modularization of gratings using CAMFR and planewave expansion.

The upward propagating plane wave spectra of the ILG ($\boldsymbol{t_{A\to B}}$ in Eqn. 3) and FSG ($\boldsymbol{t_{C\to D}}$ in Eqn. 4) depicted in are found by computing the Discrete Fourier Transform Eqn. 2 of the E_z field in the channel above the gratings. E_z is found using the Eigenmode Solver CAMFR. Reciprocity is exploited to reverse the flow of optical power in calculation of $\boldsymbol{t_{C\to D}}$.

$$a_i[\Delta\theta_i] = \sqrt{\frac{\Delta k_i}{2\pi\eta}} \sum_{m=0}^{M} E_z[x_m] e^{j\Delta k_i \cdot x_m} \qquad (2)$$

$$\boldsymbol{t_{A\to B}} = \begin{pmatrix} t_{A\to B}^{(\mathbf{1})} \\ \cdots \\ t_{A\to B}^{(N)} \end{pmatrix} \qquad (3) \qquad\qquad \boldsymbol{t_{C\to D}} = \begin{pmatrix} t_{D\to C}^{(\mathbf{1})} \\ \cdots \\ t_{D\to C}^{(N)} \end{pmatrix}^{H} \qquad (4)$$

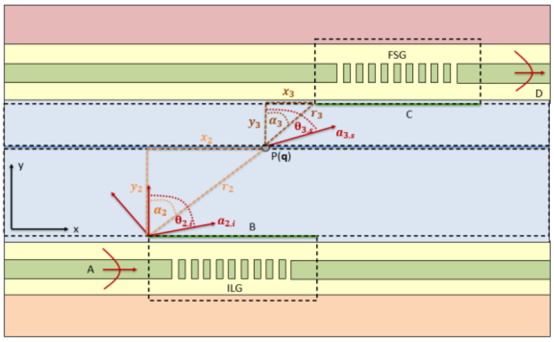

Figure 4 TMM modularization of microfluidic channel using plane wave phase rotations

Figure 4 depicts the TMM modularization of the microfluidic channel, assumed to be a lossless, linear, homogeneous dielectric. Propagation of a plane wave $'\boldsymbol{a}'$ along a displacement '$\boldsymbol{r}'$' within the channel induces a phase rotation on the plane wave calculated using Eqn. 5 and 6. The phase rotations for a plane wave spectrum can be computed and used in Eqns. 7 and 8 to populate the channel transmission matrices $\boldsymbol{t_{A\rightarrow P}}$ in Eqn. 9 and $\boldsymbol{t_{P\rightarrow D}}$ in Eqn. 10. Translation of components such as the FSG or bead within the channel corresponds to the generation of the new $\boldsymbol{t_{A\rightarrow P}}$ and $\boldsymbol{t_{P\rightarrow D}}$ matrices, a computationally inexpensive operation.

$$\emptyset_{2,\ i} = \boldsymbol{k}_{2,\ i} \cdot \boldsymbol{r}_2 = \frac{2\pi n_w}{\lambda}\sqrt{x_2 + y_2}cos(\theta_{2,\ i} - \alpha_{2,\ i}) \qquad (5)$$

$$\emptyset_{3,\ s} = \boldsymbol{k}_{3,\ s} \cdot \boldsymbol{r}_3 = \frac{2\pi n_w}{\lambda}\sqrt{x_2 + y_2}cos(\theta_{3,\ i} - \alpha_{3,\ i}) \qquad (6)$$

$$t^{(i)}_{B\rightarrow P} = e^{-j\emptyset_{2,\ i}} \qquad (7) \qquad\qquad t^{(s)}_{P\rightarrow C} = e^{-j\emptyset_{3,\ s}} \qquad (8)$$

$$\boldsymbol{t_{B\rightarrow P}} = \begin{pmatrix} t^{(\mathbf{1})}_{B\rightarrow P} & \cdots & 0 \\ \vdots & \ddots & \vdots \\ 0 & \cdots & t^{(N)}_{B\rightarrow P} \end{pmatrix} \qquad \boldsymbol{(9)} \qquad \boldsymbol{t_{P\rightarrow C}} = \begin{pmatrix} t^{(\mathbf{1})}_{P\rightarrow C} & \cdots & 0 \\ \vdots & \ddots & \vdots \\ 0 & \cdots & t^{(N)}_{P\rightarrow C} \end{pmatrix} \qquad \boldsymbol{(10)}$$

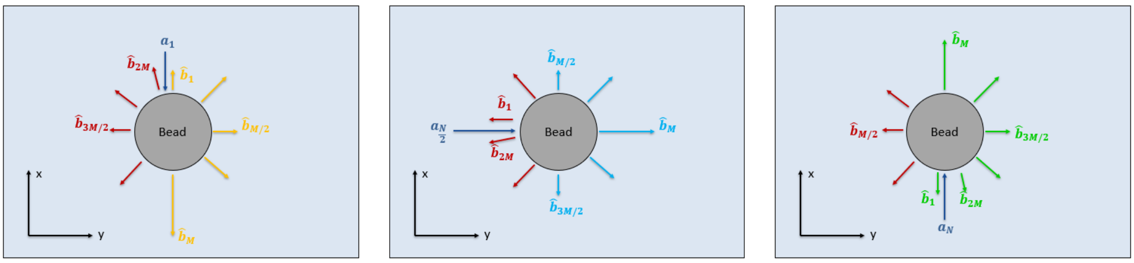

Figure 5 TMM modularization of the bead via Mie Theory

The bead transmission matrix $\boldsymbol{t_P}$ is found by modelling the bead as a lossless dielectric cylinder in 2D, for which Mie Theory can be used to calculate the fields scattered due a plane wave excitation. The circular symmetry is exploited to find the upwards (rightwards in Figure 5) propagating spectra for various incident plane wave angles as in which then populate the rows of the $\boldsymbol{t_P}$ matrix in Eqn. 11.

$$\boldsymbol{t_P} = \begin{pmatrix} \hat{b}_M & \cdots & \hat{b}_1 \\ \vdots & \ddots & \vdots \\ \hat{b}_1 & \cdots & \hat{b}_M \end{pmatrix} \qquad \boldsymbol{(11)}$$

Validation and Optimization

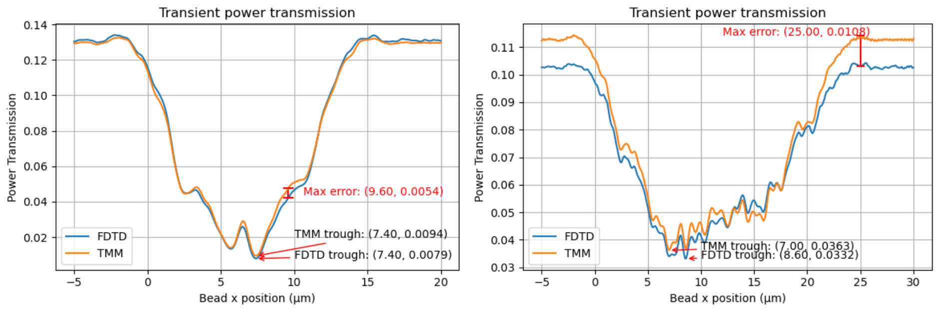

Figure 6 Comparing performance of TMM and Lumerical FDTD in transient simulation

Figure 6 depicts transient power transmission simulated while sweeping the bead position by both a 2881 plane wave TMM (using Eqn. 1) and Lumerical FDTD. Gratings with a period of $\Lambda_{FSG} = \Lambda_{ILG} = 490nm$, relative FSG position of $x_{FSG} = 3.1\mu m$ and consisting of 21 periods and 41 periods were simulated. The similar shape, trough position and small error indicate sufficiently close agreement between the TMM and FDTD simulations. The simulations took the TMM 15s and 53s to complete, a four to five order-of-magnitude reduction in computation time compared to the, on average, 70 and 671 hours it takes for the FDTD solver to complete on the same computational hardware.

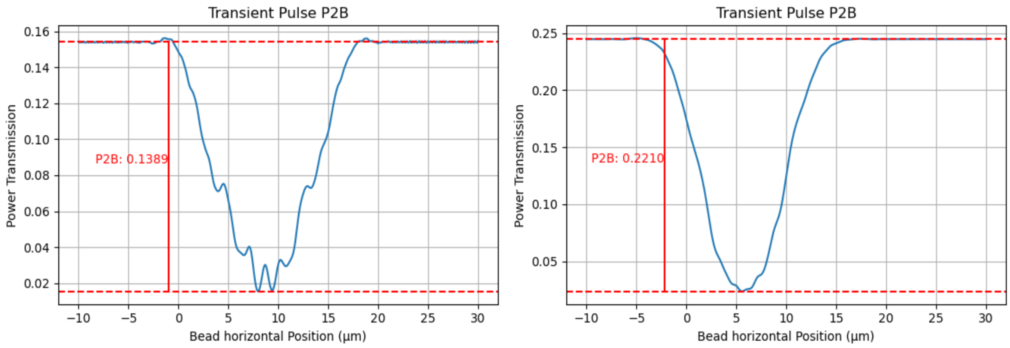

Figure 7 Transients and P2B of optimized linear (left) and linearly apodized (right) grating configurations

The TMM is integrated into a Bayesian Optimization by Gaussian Process scheme for the efficient optimization of P2B. The scheme yields a (a) uniform grating consisting of 24 periods, $\Lambda_{FSG} = \Lambda_{ILG} = 511nm$ and $\boldsymbol{x_{FSG}} = 5.323\mu m$ and (b) a linearly apodized grating consisting of 39 periods, $\Lambda_{FSG} = \Lambda_{ILG} = 423nm$, $x_{FSG} = -3.959\mu m$ and a linear apodization strength of $R = 0.0135\mu m^{-1}$ depicted in Figure 7. The linearly apodized grating yields an approximately 2dB improvement in P2B on the uniform grating.

References

[1] S. Jooken, K. Zinoviev, G. Yurtsever, et al., "On-chip flow cytometer using integrated photonics for the detection of human leukocytes," Sci. Reports 14, 10921 (2024).